JOURNAL OF AIRCRAFT
Vol. 31, No. 6, November–December 1994

Limit Cycle Phenomena in Computational Transonic Aeroelasticity

Kenneth A. Kousen*
United Technologies Research Center, East Hartford, Connecticut 06108
and
Oddvar O. Bendiksen†
University of California, Los Angeles, Los Angeles, California 90024

Limit cycle behavior has been observed in past transonic flutter calculations by the authors, using a two degree-of-freedom typical section model coupled to an unsteady Euler equations solver. In this article, the structural nonlinearity of freeplay has been added to the typical section model, and its effects on the dynamic stability problem are assessed. In addition, limit cycle behavior in the swept-wing model of Isogai is demonstrated and related to the observed presence of multiple flutter points in the transonic dip region.

Nomenclature

a = location of elastic axis
c = $2b$, airfoil chord
e = total energy
h = plunge displacement at elastic axis, positive down
K_h = typical section bending stiffness
K_α = typical section torsional stiffness
k = $\omega b/U$, reduced frequency
M = Mach number
m = mass per unit span
p = pressure
$\boldsymbol{Q}$ = vector of generalized forces
$\boldsymbol{q}$ = vector of generalized coordinates
R = ω_h/ω_α
r_α = nondimensional radius of gyration about elastic axis
t = time
U_∞ = freestream velocity at upstream infinity
$\bar{U}$ = $U_\infty/b\omega_\alpha$, reduced velocity
u, v = velocities in x, y directions
x_α = nondimensional c.g.-elastic axis offset
α = torsional deflection, positive nose up
α_s = torsional free-play, Fig. 2
γ = ratio of specific heats
η_r = rth normal coordinate
μ = $m/\pi\rho b^2$, mass ratio
ρ = air density
τ = $\omega_\alpha t$, nondimensional time
$\boldsymbol{\phi}_r$ = rth normal mode vector
ω = circular frequency, rad/s
ω_h = uncoupled frequency in bending
ω_α = uncoupled frequency in torsion

Introduction

LIMIT cycle flutter has been previously observed in nonlinear time-marching, Euler-based flutter calculations in the transonic operating regime.[1–3] As long as separation does not occur in the flow, the Euler equations provide a reasonable aerodynamic model for transonic flutter calculations, including the modeling of aerodynamic nonlinearities that can result in limit cycle behavior. A large-amplitude aeroelastic model, however, should have the capability of modeling both structural as well as aerodynamic nonlinearities. In this article, the typical section model used in Refs. 1–3 has been modified to include the structural nonlinearity of free-play in the torsional degree of freedom (DOF). The primary purpose of this article is to present preliminary results showing the effects of free-play on the observed limit cycle behavior in the transonic regime, where strong aerodynamic nonlinearities are present.

The influence of structural nonlinearities on aeroelastic stability has previously been examined in Refs. 4–10. In general, these studies have involved simple aerodynamic models, based either on analytic closed-form solutions (where available), or on linearized versions of more elaborate theories. Analytic studies based on Theodorsen function incompressible aerodynamics and nonlinear structural models have been carried out by Woolston et al.,[4] Shen,[5] Shen and Hsu,[6] and Breitbach.[7] These studies used simple dynamic systems that could be represented mathematically and analyzed using harmonic balance methods, and contained only a single concentrated nonlinearity. Lee[8] extended the analysis to multiple nonlinearities, and Laurenson et al.[9] included the effect of higher harmonic terms in the analysis. Lee[8] calculated the flutter boundary for a theoretical model studied experimentally by McIntosh et al.,[10] containing freeplay, hysteresis, and preloads, and observed a subcritical bifurcation.

It was observed in Ref. 1 that limit cycle flutter behavior is an inherent transonic phenomenon, brought about by aerodynamic nonlinearities inherent in mixed subsonic-supersonic flows containing strong shocks. Another unusual transonic phenomenon that has been recorded previously is the presence of multiple flutter points in the swept wing model problem of Isogai.[11] He introduced a two-dimensional analog for a swept wing by examining the dynamic response of streamwise sections of a swept wing and adjusting the typical section structural parameters to model the observed bending-torsion motion of the outboard section of the wing. For the wing studied by Isogai, this resulted in an effective elastic axis a full chord-length ahead of the leading edge of the airfoil, and a ratio of the uncoupled natural frequencies R equal to one. In Ref. 12, he then used LTRAN2[13] to calculate the flutter boundary for this model, which exhibited a pronounced "transonic dip" phenomenon. The flutter boundary in the transonic dip region is characterized by a drop in the flutter speed for

Presented as Paper 89-1185 at the AIAA/ASME/ASCE/AHS/ASC 30th Structures, Structural Dynamics, and Materials Conference, Mobile, AL, April 3–5, 1989; received May 10, 1990; revision received June 22, 1993; accepted for publication Feb. 3, 1994.

*Research Engineer. Member AIAA.
†Associate Professor, Department of Mechanical, Aerospace and Nuclear Engineering. Member AIAA.

increasing transonic Mach numbers, followed by a sharp recovery.[12,14-16] At Mach numbers slightly lower than this recovery, several researchers[2,15,17] have observed that an increase in the reduced velocity can result in multiple flutter points.

The second purpose of this article is to re-examine these results, with the intention of demonstrating that the multiple flutter points are bounds of "pockets" of limit cycles. In particular, we show that a stable system at a low reduced velocity can go unstable as the reduced velocity is increased, and then become stable once again, and finally unstable in a different flutter mode.

Theoretical Models and Numerical Solution

Structural Model

Figure 1 shows the typical section model in a uniform freestream. The airfoil DOFs are the pitch angle α between the airfoil chord and the freestream, positive nose up, and the plunge displacement h, measured positive downwards at the elastic axis (EA). The plunge displacement is nondimensionalized with respect to the airfoil semichord b. The pitching and plunging stiffnesses are modeled by linear springs attached at the EA. The relevant nondimensional parameters for the coupled problem are the elastic axis location a, the radius of gyration about the elastic axis r_α, the mass ratio $\mu = m/\pi\rho_\infty b^2$, the frequency ratio $R = \omega_h/\omega_\alpha$ of the uncoupled natural frequency in plunge to that in pitch, the Mach number M, and the reduced velocity $\bar{U} = U_\infty/b\omega_\alpha$. In addition, time is nondimensionalized with respect to the uncoupled natural frequency of the structure in pitch, i.e., $\tau = \omega_\alpha t$.

In terms of these dimensionless quantities, the equations of motion for the aeroelastic system are

$$\frac{d^2}{d\tau^2}\left(\frac{h}{b}\right) + x_\alpha \frac{d^2\alpha}{d\tau^2} + \frac{\omega_h^2}{\omega_\alpha^2}\frac{h}{b} = -\frac{\bar{U}^2}{\pi\mu} C_L \tag{1}$$

$$x_\alpha \frac{d^2}{d\tau^2}\left(\frac{h}{b}\right) + r_\alpha^2 \frac{d^2\alpha}{d\tau^2} + r_\alpha^2\alpha = \frac{2\bar{U}^2}{\pi\mu} C_M \tag{2}$$

where C_L and C_M are the nondimensional lift and moment coefficients, respectively. These equations can be written in the form

$$M\ddot{q} + Kq = Q \tag{3}$$

where M and K are mass and stiffness matrices, respectively, q is the vector of independent variables, and Q is the vector of generalized forces.

The equations are transformed into normal coordinates for integration. This approach can be generalized to a more realistic Rayleigh-Ritz, Galerkin, or finite element formulation of the flutter problem of a wing structure. In such cases, the number of DOF can be quite large, and contain many high-frequency components that are not physically relevant to the aeroelastic problem. A truncated model based on the normal mode method is then useful. By solving the free vibration problem, the natural frequencies ω_r and normal modes ϕ_r can be determined. If these are then ordered in the direction of increasing frequency, $\omega_1 \le \omega_2 \le \cdots$, the first N modes ϕ_1, $\phi_2, \ldots, \phi_N$ are kept in the flutter analysis. The flutter mode is then restricted to lie in the subspace spanned by the first N eigenvectors, i.e.,

$$q = \sum_{r=1}^{N} \eta_r(t)\phi_r \tag{4}$$

and a reduced N-DOF problem involving the normal coordinates $\eta_r(t)$ is solved. This process decouples the left sides of the equations of motion, so that now the only coupling between normal coordinates occurs through the generalized aerodynamic forces.

The equations in normal coordinates become

$$\ddot{\eta} + (\omega_r^2/\omega_\alpha^2)\eta_r = F_r \tag{5}$$

for $r = 1, 2, \ldots, N$, where

$$F_r = \phi_r^T \cdot Q \tag{6}$$

Viscous-type structural damping is readily added to the model by including the term $2(\omega_r/\omega_\alpha)\zeta_r\dot{\eta}_r$ on the left side of Eq. (5), where ζ_r is the damping ratio of the rth mode.

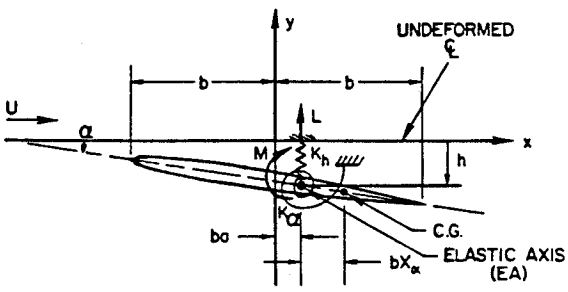

Fig. 1 Typical section model.

Aerodynamic Model

Many different numerical schemes have been devised for the various aerodynamic approximations possible for unsteady transonic flows. An excellent review of the field is provided in Ref. 18. The aerodynamic model used here is based on a finite volume discretization of the unsteady Euler equations, which represent the conservation of mass and the balance of momentum and energy in an inviscid compressible fluid. The formation and subsequent motion of shock waves have been found to be of crucial importance in the aeroelastic problem,[1,19] so that the aerodynamic equations are placed in weak conservation form to easily handle discontinuities in the flow.

In the finite volume scheme developed by Jameson and Venkatakrishnan,[20,21] the two-dimensional Euler equations are written in the following integral form on a moving mesh:

$$\frac{\partial}{\partial t}\int_\Omega W\, dx\, dy + \int_{\partial\Omega} (f\, dy - g\, dx) = 0 \tag{7}$$

where Ω is an element area with (moving) boundaries $\partial\Omega$ and

$$W = \begin{Bmatrix} \rho \\ \rho u \\ \rho v \\ \rho e \end{Bmatrix}, \qquad f = \begin{Bmatrix} \rho(u - x_t) \\ \rho u(u - x_t) + p \\ \rho v(u - x_t) \\ \rho e(u - x_t) + pu \end{Bmatrix} \tag{8}$$

$$g = \begin{Bmatrix} \rho(v - y_t) \\ \rho u(v - y_t) \\ \rho v(v - y_t) + p \\ \rho e(v - y_t) + pv \end{Bmatrix} \tag{9}$$

In these equations, W is the vector of independent variables, f is the x-direction flux of mass, momentum, and energy, and p, ρ, u, v, and e are the pressure, density, Cartesian velocity components and energy, respectively. The quantities x_t and y_t are the velocity components of the moving boundary $\partial\Omega$. The pressure p can be eliminated by using the relation for e for a perfect gas

$$e = p/[(\gamma - 1)\rho] + \tfrac{1}{2}(u^2 + v^2) \tag{10}$$

These equations are solved on a nondeformable C-mesh of quadrilateral elements rigidly attached to the airfoil. Equation

(7) is applied to each cell (i, j) of the mesh, resulting in a system of ordinary differential equations of the form

$$\frac{d}{dt}(S_{ij}W_{ij}) + Q_{ij} = 0 \tag{11}$$

where S_{ij} is the area of cell (i, j), and Q_{ij} is the net flux out of cell (i, j). A dissipative term is added to prevent odd-even decoupling in the mesh and to suppress spurious oscillations. The dissipative operator used in this article was developed by Jameson and Baker,[22] and is composed of a careful blend of second- and fourth-order differences of the independent variables. The dissipative term D_{ij} enters the semidiscretized equations as follows:

$$\frac{d}{dt}(S_{ij}W_{ij}) + Q_{ij} - D_{ij} = 0 \tag{12}$$

These equations are then integrated forward in time using a hybrid five-stage Runge-Kutta scheme of the type suggested by Jameson et al.[23] For computational efficiency, the dissipative operator is evaluated during the first two stages only. Nonreflecting boundary conditions based on the work of Hedstrom,[24] as adapted by Venkatakrishnan,[21] are used in the far field, and the flow tangency boundary condition is evaluated at the instantaneous position of the airfoil surface.

Coupled Integration

Integration of the coupled fluid/structural equations of motion is based on a convolution integral solution of the forced response problem, obtained by assuming that the right side terms of Eq. (5) are functions of time only. Making use of the linearity of the structural model, one can solve the forced vibration equations by using Laplace transforms, to reach

$$\eta_r(t) = \eta_r(0)\cos\omega_r t + \frac{1}{\omega_r}\dot{\eta}_r(0)\sin\omega_r t + \frac{1}{\omega_r}\int_0^t F_r(T)\sin[\omega_r(t - T)]\,dT \tag{13}$$

Rather than carry the initial conditions along throughout the time integration, an alternative is to express $\eta_r(t^{n+1})$ in terms of $\eta_r(t^n)$. If Δt is defined by

$$\Delta t = t^{n+1} - t^n \tag{14}$$

then the discretized equation for $\eta_r(t^{n+1})$ can be written as

$$\eta_r(t^{n+1}) = \eta_r(t^n)\cos\omega_r\Delta t + \frac{1}{\omega_r}\dot{\eta}_r(t^n)\sin\omega_r\Delta t + \frac{1}{\omega_r}\int_0^{\Delta t} F_r(T)\sin[\omega_r(t - T)]\,dT \tag{15}$$

If $F_r(t)$ can be assumed to be piecewise linear over each time step, then the convolution integral can be expanded and evaluated exactly. The aerodynamic integrator discussed above chooses a time step based on the Courant-Friedrichs-Lewy (CFL) condition. It turns out that this time step is sufficiently small so that the assumption of linearity in $F_r(t)$ is reasonable. $F_r(t)$ is therefore assumed to be of the form

$$F_r(t) = F_r(t^n) + \left[\frac{\Delta F_r}{\Delta t}\right]_n (t - t^n) \tag{16}$$

over the interval $t^n \le t \le t^{n+1}$, where

$$\left[\frac{\Delta F_r}{\Delta t}\right]_n = \frac{F_r(t^{n+1}) - F_r(t)}{t^{n+1} - t^n} \tag{17}$$

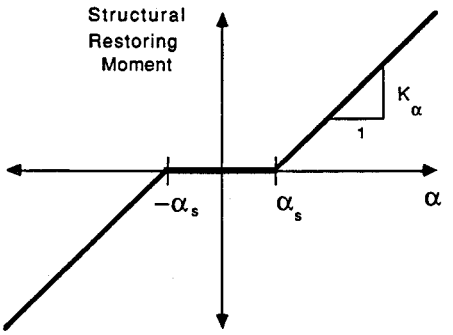

Fig. 2 Nonlinear torsional resistance curve.

Finally, since the value of F_r at time t^{n+1} is unavailable during the current time step, it is approximated by assuming that

$$\left[\frac{\Delta F_r}{\Delta t}\right]_n = \left[\frac{\Delta F_r}{\Delta t}\right]_{n-1} \tag{18}$$

Note that in the free-play region, somewhat different equations must be used since the natural frequency in torsion is zero. The resulting equations are easily determined and implemented in the code.

Results

In general, the results presented in this article were calculated by first computing a converged steady flow solution about the airfoil, then forcing the airfoil in pitch about the elastic axis for three to five complete cycles with an amplitude of either 0.1 or 4.0 deg, followed by release. The subsequent aeroelastic response of the model was obtained by a time-marching solution of the aeroelastic equations. The steady Euler solution was determined using the steady portion of the original unsteady Euler solver, which also contained provisions for using multigrid. Generally, a time history containing 40–60 complete cycles of oscillations was computed.

Except as noted, the solutions were determined on a 96 × 16 C-mesh that moved with the airfoil. The coordinates for the symmetric NACA 64A010 and NACA 64A006 airfoils were taken from Bland.[25]

Effect of Torsional Freeplay

An example of a structural nonlinearity that can be readily included in the present model is torsional free-play, which could represent a loose hinge or linkage backlash in a control system. Its effects on the flutter boundary of an airfoil in an incompressible flow were explored by Lee and Desrochers.[26] In this model, the linear torsional moment function is replaced by the nonlinear function shown in Fig. 2. Any pitch displacement between $-\alpha_s$ and $+\alpha_s$ would result in a torsional resistance of 0. Free-play modifies the aeroelastic equations of motion by changing Eq. (2) to

$$x_\alpha\frac{d^2}{d\tau^2}\left(\frac{h}{b}\right) + r_\alpha^2\frac{d^2\alpha}{d\tau^2} + r_\alpha^2 f(\alpha) = \frac{2\bar{U}^2}{\pi\mu}C_M \tag{19}$$

where the piecewise linear function $f(\alpha)$ is given by

$$\begin{aligned} f(\alpha) &= \alpha - \alpha_s \qquad \alpha > \alpha_s \\ f(\alpha) &= 0 \qquad -\alpha_s < \alpha < \alpha_s \\ f(\alpha) &= \alpha + \alpha_s \qquad \alpha < -\alpha_s \end{aligned} \tag{20}$$

This was implemented into the code in the following manner. Outside the zero torsional resistance region, Eq. (2) can be written as

$$x_\alpha\frac{d^2}{d\tau^2}\left(\frac{h}{b}\right) + r_\alpha^2\frac{d^2\alpha}{d\tau^2} + r_\alpha^2\alpha = \frac{2\bar{U}^2}{\pi\mu}C_M \pm r_\alpha^2\alpha_s \tag{21}$$

where the plus sign is used when $\alpha > \alpha_s$, and the minus sign is used when $\alpha < -\alpha_s$. The convolution integral solution can then be used by simply adding the appropriate constant term into the generalized forcing function. In between $-\alpha_s$ and α_s, however, the eigenvalues and eigenvectors of the resulting free vibration problem are different (since the torsional resistance is zero), and so care must be taken to adjust ω_r and ϕ_r accordingly.

To examine the effect of structural free-play on transonic flutter, a relatively well-understood case from Ref. 1 was chosen. The system is a NACA 64A010 airfoil at Mach 0.87 with structural parameters

$$a = -0.2$$

$$x_\alpha = 0.2$$

$$r_\alpha^2 = 0.29$$

$$R = 0.34335$$

$$\mu = 60$$

This system is similar to one studied by Ashley.[19] This system at Mach 0.87 undergoes a supercritical bifurcation to a set of stable limit cycles, whose character becomes increasingly distorted as $\bar{U}$ is increased. An example of this case is shown in Fig. 3, which shows the pitch time history and phase plane plots for the case $\bar{U} = 2.0$. The slow approach of the system to relatively small-amplitude limit cycles indicates that this system is near its linear flutter point (which was found to be approximately 1.9).

Free-play was then added to the torsional spring by setting $\alpha_s = 1$ deg, and the new coupled system was integrated forward in time for a range of $\bar{U}$ values. Some results for this

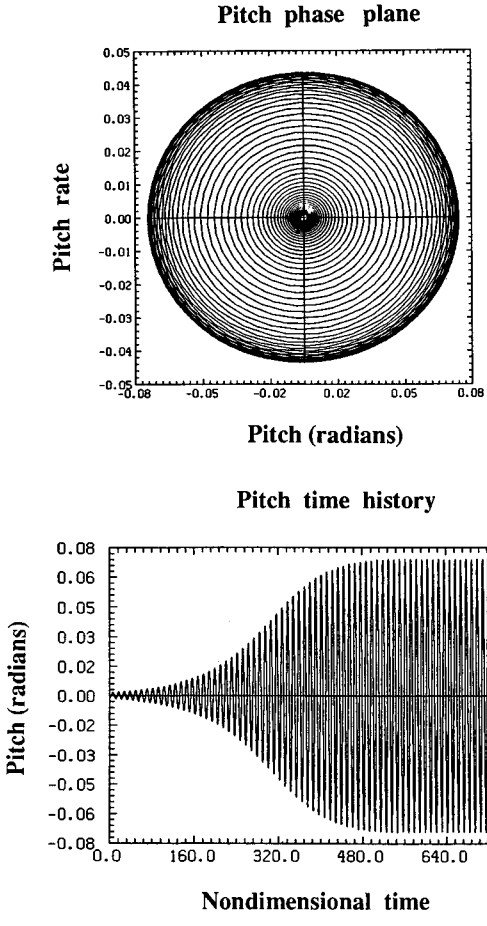

Fig. 3 Limit cycle oscillations without free-play ($M = 0.87$, $\bar{U} = 2.0$).

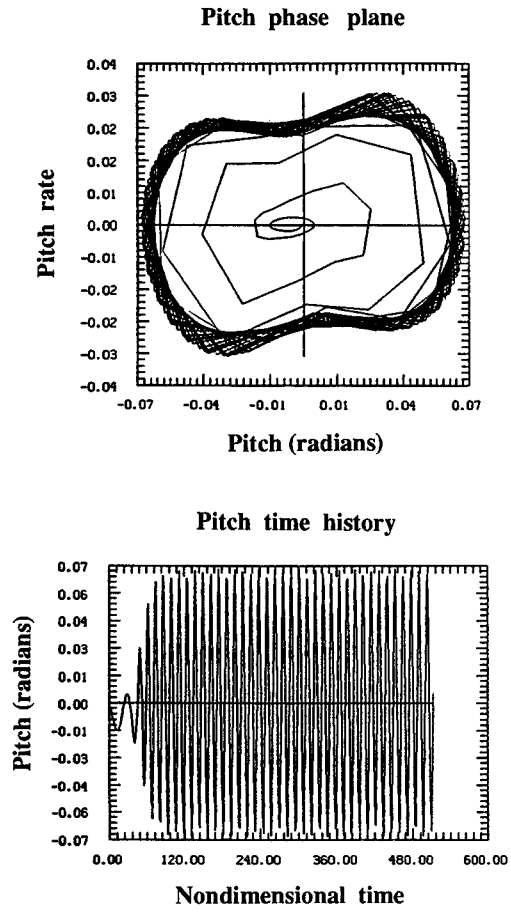

Fig. 4 Free-play pitch limit cycle for $\bar{U} = 1.5$.

situation are shown in Figs. 4 and 5. Figure 4 shows the pitch time history and phase plane trajectory for a reduced velocity of 1.5. Note the obvious distorted character of the phase plane, indicating the presence of higher frequency components in the solution.

Decreasing $\bar{U}$ in order to locate the linear stability point resulted in limit cycles of lesser amplitudes at reduced velocities of 1.4 and 1.3. Below 1.3, the initial forcing amplitude of the airfoil was increased from 0.1 to 4.0 deg to guarantee that the system began its released oscillations outside the freeplay region. Later checks indicated that the dependence of the limit cycle on the initial amplitude was very weak.

Using the 4.0-deg forcing, time integrations were performed for reduced velocities from 1.1 down to 0.2. Figure 5 shows pitch time history and phase plane plots at $\bar{U} = 0.6$, which is just above the bifurcation point. For reduced velocities of 0.5 and below, the system does not enter a limit cycle, but rather travels to the stable equilibrium position defined by equating the static aerodynamic and structural restoring forces and moments. This type of "weak divergence" behavior has been observed for other aeroelastic systems (without free-play) in Ref. 1.

A bifurcation diagram for the free-play cases is shown in Fig. 6. Note that the limit cycles resulting from the 4.0-deg forcing appear to fall on the same curve as those that resulted from 0.1-deg forcing. To verify that the amplitude dependence was minimal, a case was run at a reduced velocity of 1.7 with 4.0 deg of forcing. The resulting limit cycle amplitude differed from the one found with 0.1-deg forcing by less than 2%.

Note that the bifurcation curve contains a discontinuity at around $\bar{U} = 0.5$. The lack of torsional rigidity in the free-play region prevents the formation of pitch limit cycles at reduced velocities where the resulting pitch limit cycle amplitude might be expected to be less than 1.0 deg. The overall form of this curve is qualitatively similar to an analogous

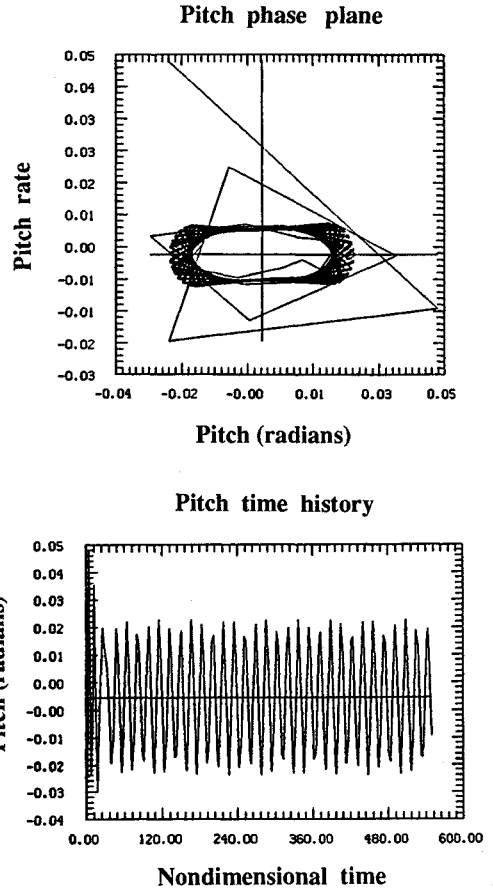

Fig. 5 Free-play pitch limit cycle for $\bar{U} = 0.6$.

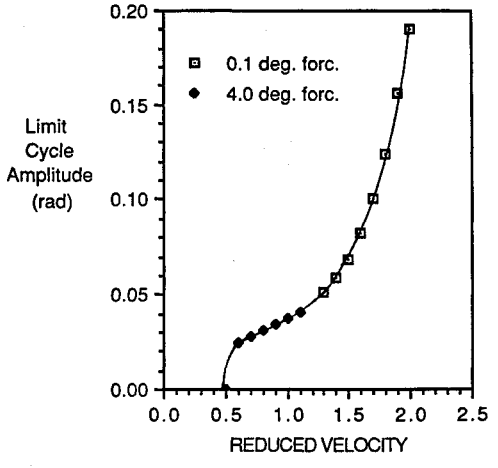

Fig. 6 Free-play bifurcation diagram.

figure in Breitbach,[7] in his studies of control surface free-play in incompressible flow.

Also of interest is the fact that the linear flutter point of the system has dropped significantly, from $\bar{U}$ of about 1.9 without free-play, to around 0.5 with the free-play. In this sense, the addition of free-play has been highly destabilizing.

Isogai Swept-Wing Model

Figure 7 shows the flutter boundaries computed for a NACA 64A010 airfoil with parameters

$$a = -2.0$$

$$x_\alpha = 1.8$$

$$r_\alpha^2 = 3.48$$

$$R = 1.0$$

$$\mu = 60.0$$

In order to facilitate comparisons with previous versions of this figure that have appeared in the literature, the flutter boundary is plotted in terms of the "speed index" $\bar{U}/\sqrt{\mu}$ vs M. Note that there is a sharp bend-back in the flutter boundary at about Mach 0.90–0.91 (depending on mesh density used in calculations), and multiple flutter points exist over a small range of Mach numbers below the bend-back point. For example, on a 96 × 16 mesh, our calculations predict both an "upper" and a "lower" flutter point at Mach 0.90 (see Fig. 7).

Figure 8 is a new version of this figure containing data from the present code only, identifying the flutter modes that occur. The dashed lines in this diagram represent the qualitative form the curves are expected to follow, based on the transonic small disturbance (TSD) studies of Weatherill and Ehlers.[15] Of interest is the change in the flutter mode of the system with increasing reduced velocity at a constant Mach number. The first (lower frequency) coupled mode for this structure is dominated by the plunging free vibration mode. Isogai in Ref. 12 observed that at the bottom of the transonic dip, the phase difference between the pitching and plunging oscillations went to zero, and identified this mode as a single-DOF associated with a pitching oscillation about a point ahead of the airfoil. Weatherill and Ehlers[15] then identified this with the first pitch-

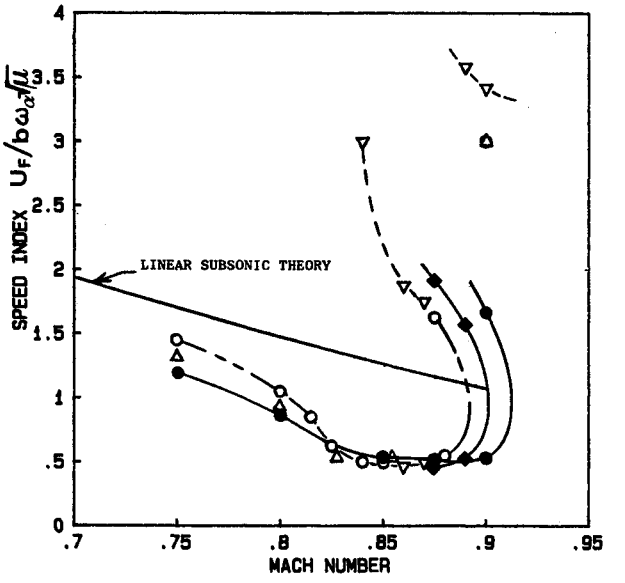

Fig. 7 Flutter boundary of swept NACA 64A010 model. ●—present code, 96 × 16 mesh; ◆—present code, 192 × 32 mesh; ○—HYTRAN2[14]; ▽—OPTRAN2[15]; △—EXTRAN2.[27]

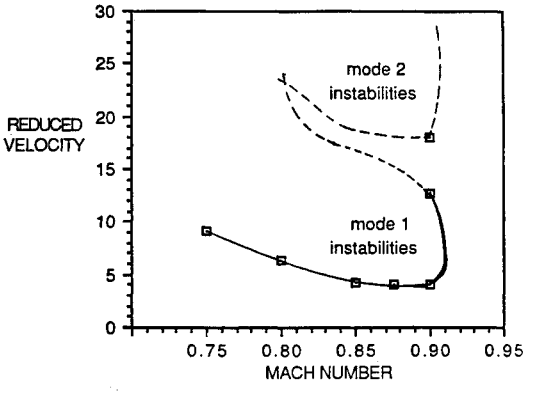

Fig. 8 Flutter boundary of swept NACA 64A010 model in terms of reduced velocity.

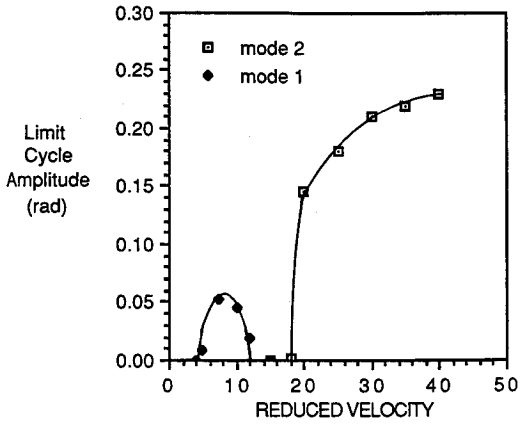

Fig. 9 Bifurcation diagram for swept NACA 64A010 model.

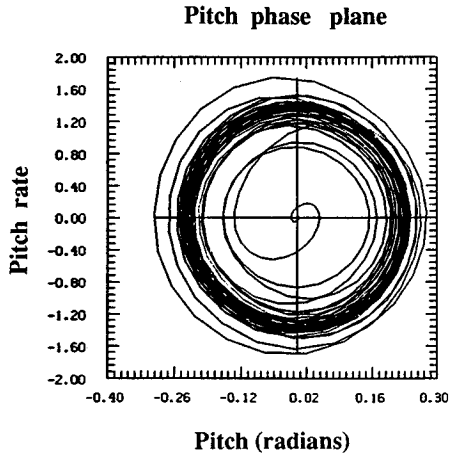

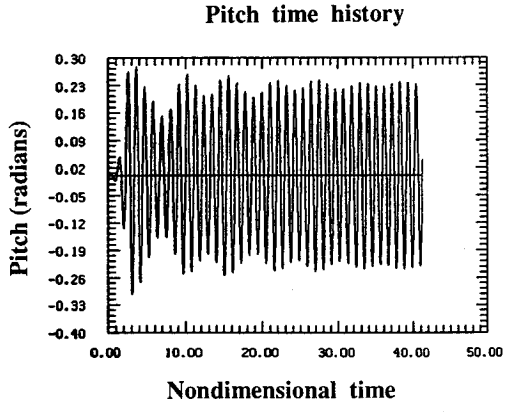

Fig. 10 Limit cycle flutter, $\bar{U} = 35.0$.

ing mode of the overall wing. The second (higher frequency) coupled mode is more balanced between the first and second free vibration modes, and more closely resembles pitching of the system about a point between the leading edge and the elastic axis.

At a constant Mach number of 0.90, a series of time-integrations was performed at increasing reduced velocities from 0 to 70. In each case, the integration was continued until the motion of the system either began limit cycle oscillations or decayed to zero. When limit cycle oscillations did occur, the resulting steady-state amplitude and oscillation mode were noted. The results are shown in the bifurcation diagram given in Fig. 9, which shows the pitch limit cycle amplitude vs reduced velocity. For $\bar{U}$ values below 4, the system approaches the stable equilibrium point at 0. Between 4–13, the system is characterized by a series of limit cycles that first increase and then decrease in amplitude with increasing reduced velocity. In these cases, the limit cycle oscillations are in the

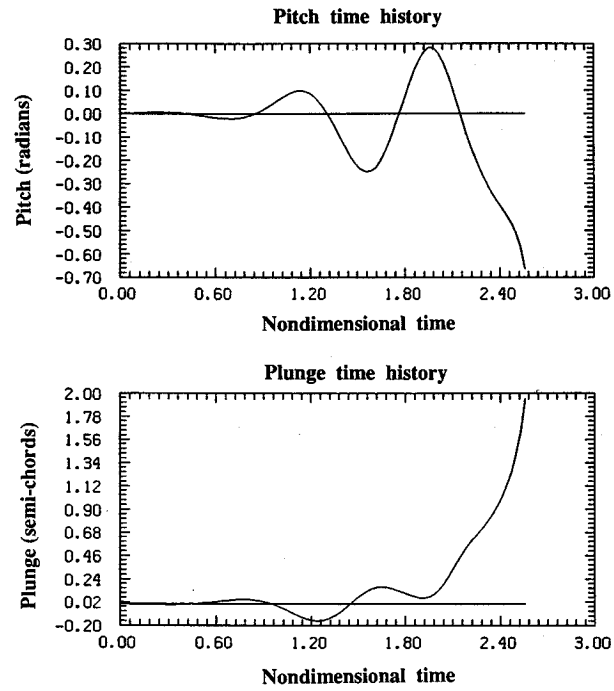

Fig. 11 Strong divergence, $\bar{U} = 50.0$.

first mode defined above. At slightly above 13, the system once again returns to the equilibrium point at 0. Observing Fig. 9, it is seen that these limit cycle oscillations are contained in the bend-back region of Figs. 7 and 8, the boundaries of which are now understood to be the beginning and ending of this "pocket" of limit cycles.

Raising the reduced velocity further eventually results in second-mode limit cycle oscillations, whose amplitudes increase monotonically with increasing reduced velocity as shown. The second mode set of limit cycles appears to take the form of a supercritical bifurcation. Figure 10 shows the pitch time history and phase plane curves for the case $\bar{U} = 35$, $M = 0.90$. From the time histories, it is apparent that higher frequency terms are present in the solution, but are gradually decaying away, with the result being the limit cycles shown.

Above a reduced velocity of $\bar{U} = 50.0$, the system exceeds a strong divergence condition, with the results shown in Fig. 11. Note that in comparison with the approach to limit cycles seen previously, this divergence is extremely rapid.

Conclusions

The primary conclusions to be drawn from this study can be summarized as follows:

1) Adding torsional free-play to a typical section model in transonic flow proved strongly destabilizing. In the case studied (± 1-deg free-play), the linear flutter speed decreased by nearly 75%, and limit cycle amplitudes for $\bar{U}$ values above the flutter point were larger than the corresponding cases without free-play.

2) In the Isogai swept-wing model at Mach 0.90 and reduced velocities above the bend-back of the flutter curve, the flutter mode changes from the first (lower frequency) mode to the second (higher frequency) mode.

3) A bifurcation diagram for the NACA 64A010 airfoil in this swept configuration reveals that the bend-back region contains a pocket of limit cycles, whose amplitudes first increase and then decrease to 0. Limit cycles for the second mode instability form a supercritical bifurcation.

4) For the NACA 64A010 airfoil at Mach numbers slightly beyond the bend-back, the system's oscillations are strongly damped for $\bar{U}$ values from 0 to nearly 70, at which point a strong divergence condition is exceeded.

References

[1]Kousen, K. A., and Bendiksen, O. O., "Nonlinear Aspects of the Transonic Aeroelastic Stability Problem," *Proceedings of the AIAA/ASME/ASCE/AHS 29th Structures, Structural Dynamics, and Materials Conference* (Williamsburg, VA), AIAA, Washington, DC, 1988, pp. 760–769.

[2]Bendiksen, O. O., and Kousen, K. A., "Transonic Flutter Analysis Using the Euler Equations," AIAA Paper 87-0911, April 1987.

[3]Kousen, K. A., "Nonlinear Phenomena in Computational Transonic Aeroelasticity," Ph.D. Dissertation, Dept. of Mechanical and Aerospace Engineering, Princeton Univ., Princeton, NJ, Jan. 1989.

[4]Woolston, D. S., Runyan, H. W., and Andrews, R. E., "An Investigation of Effects of Certain Types of Structural Nonlinearities on Wing and Control Surface Flutter," *Journal of the Aeronautical Sciences*, Vol. 24, Jan. 1957, pp. 57–63.

[5]Shen, S. F., "An Approximate Analysis of Nonlinear Flutter Problems," *Journal of the Aerospace Sciences*, Vol. 28, Jan. 1959, pp. 25–32.

[6]Shen, S. F., and Hsu, C. C., "Analytical Results of Certain Nonlinear Flutter Problems," *Journal of the Aeronautical Sciences*, Vol. 25, Feb. 1958, pp. 136, 137.

[7]Breitbach, E. J., "Effects of Structural Nonlinearities on Aircraft Vibration and Flutter," AGARD Rept. R-665, Jan. 1978.

[8]Lee, C. L., "An Iterative Procedure for Nonlinear Flutter Analysis," *AIAA Journal*, Vol. 24, No. 5, 1986, pp. 833–840.

[9]Laurenson, R. M., Hauenstein, A. J., and Gubser, J. L., "Effects of Structural Nonlinearities on Limit Cycle Response of Aerodynamic Surfaces," AIAA Paper 86-0899, May 1986.

[10]McIntosh, S. C., Jr., Reed, R. E., Jr., and Rodden, W. P., "Experimental and Theoretical Study of Nonlinear Flutter," *Journal of Aircraft*, Vol. 18, No. 12, 1981, pp. 1057–1063.

[11]Isogai, K., "On the Transonic-Dip Mechanism of Flutter of a Sweptback Wing," *AIAA Journal*, Vol. 17, No. 7, 1979, pp. 793–795.

[12]Isogai, K., "Transonic-Dip Mechanism of Flutter of a Sweptback Wing: Part II," *AIAA Journal*, Vol. 19, No. 9, 1981, pp. 1240–1242.

[13]Ballhaus, W. F., and Goorjian, P. M., "Implicit Finite-Difference Computations of Unsteady Transonic Flows About Airfoils," *AIAA Journal*, Vol. 15, No. 12, 1977, pp. 1728–1735.

[14]Edwards, J. W., Bennett, R. M., Whitlow, W., Jr., and Seidel, D. A., "Time-Marching Transonic Flutter Solutions Including Angle-of-Attack Effects," *Journal of Aircraft*, Vol. 20, No. 11, 1983, pp. 899–906.

[15]Weatherill, W. H., and Ehlers, F. E., "A Three Degree-of-Freedom, Typical Section Flutter Analysis Using Harmonic Transonic Air Forces," AIAA Paper 83-0960, May 1983.

[16]Bland, S. R., and Edwards, J. W., "Airfoil Shape and Thickness Effects on Transonic Airloads and Flutter," *Journal of Aircraft*, Vol. 21, No. 3, 1984, pp. 209–217.

[17]Reddy, T. S. R., Srivastava, R., and Kaza, K. R. V., "The Effects of Rotational Flow, Viscosity, Thickness and Shape on Transonic Flutter Dip Phenomenon," *Proceedings of the AIAA/ASME/ASCE/AHS 29th Structures, Structural Dynamics, and Materials Conference* (Williamsburg, VA), AIAA, Washington, DC, 1988, pp. 1096–1108.

[18]Edwards, J. W., and Thomas, J. L., "Computational Methods for Unsteady Transonic Flows," AIAA Paper 87-0107, Jan. 1987.

[19]Ashley, H., "Role of Shocks in the 'Sub-Transonic' Flutter Phenomenon," *Journal of Aircraft*, Vol. 17, No. 3, 1980, pp. 187–197.

[20]Jameson, A., and Venkatakrishnan, V., "Computation of Unsteady Transonic Flows by the Solution of the Euler Equations," *AIAA Journal*, Vol. 26, No. 8, 1988, pp. 974–981.

[21]Venkatakrishnan, V., "Computation of Unsteady Transonic Flows over Moving Airfoils," Ph.D. Dissertation, Dept. of Mechanical and Aerospace Engineering, Princeton Univ., Princeton, NJ, Oct. 1986.

[22]Jameson, A., and Baker, T. J., "Solution of the Euler Equations for Complex Configurations," *Proceedings of the AIAA 6th Computational Fluid Dynamics Conference* (Danvers, MA), AIAA, New York, 1983, pp. 293–302.

[23]Jameson, A., Schmidt, W., and Turkel, E., "Numerical Solutions of the Euler Equations by Finite Volume Methods Using Runge-Kutta Time-Stepping Schemes," AIAA Paper 81-1259, June 1981.

[24]Hedstrom, G. W., "Nonreflecting Boundary Conditions for Hyperbolic Systems," *Journal of Computational Physics*, Vol. 30, Feb. 1979, pp. 222–237.

[25]Bland, S. R., "AGARD Two-Dimensional Aeroelastic Configurations," AGARD Rept. 156, Aug. 1979.

[26]Lee, B. H. K., and Desrochers, J., "Flutter Analysis of a Two-Dimensional Airfoil Containing Structural Nonlinearities," National Research Council of Canada, Rept. LR-618, May 1987.

[27]Isogai, K., "Numerical Study of Transonic Flutter of a Two-Dimensional Airfoil," National Aerospace Inst., Rept. NAL TR-617T, Tokyo, Japan, 1980.